

A Multiplicity Census of Intermediate-Mass Stars in Scorpius-Centaurus*

Markus Janson^{1,8}, David Lafrenière², Ray Jayawardhana³, Mariangela Bonavita^{3,4}, Julien H. Girard⁵, Alexis Brandeker⁶, John E. Gizis⁷

ABSTRACT

Stellar multiplicity properties have been studied for much of the range from the lowest to the highest stellar masses, but intermediate-mass stars from F-type to late A-type have received relatively little attention. Here we report on a Gemini/NICI snapshot imaging survey of 138 such stars in the young Scorpius-Centaurus (Sco-Cen) region, for the purpose of studying multiplicity with sensitivity down to planetary masses at wide separations. In addition to two brown dwarfs and a companion straddling the hydrogen burning limit we reported previously, here we present 26 new stellar companions and determine a multiplicity fraction within $0.1''$ – $5.0''$ of $21 \pm 4\%$. Depending on the adopted semi-major axis distribution, our results imply a total multiplicity in the range of ~ 60 – 80% , which further supports the known trend of a smoothly continuous increase in the multiplicity fraction as a function of primary stellar mass. A surprising feature in the sample is a distinct lack of nearly equal-mass binaries, for which we discuss possible reasons. The survey yielded no additional companions below or near the deuterium-burning limit, implying that their frequency at >200 AU separations is not quite as high as might be inferred from previous detections of such objects within the Sco-Cen region.

Subject headings: binaries: general — planetary systems — brown dwarfs

1. Introduction

The Scorpius-Centaurus (Sco-Cen) region is a young (~ 5 – 10 Myr) and relatively nearby (~ 120 – 150 pc) stellar association (de Zeeuw et al. 1999), consisting of the sub-regions Upper Scorpius (USco), Upper Centaurus Lupus (UCL), and Lower Centaurus Crux (LCC). Given its young age, in particular for USco which is the youngest sub-region, it is a promis-

ing target for direct imaging searches for wide planetary companions. Several such surveys have been conducted in USco, and have led to a surprisingly large number of detections (Lafrenière et al. 2008a; Ireland et al. 2011; Lafrenière et al. 2011), which has in turn led to the tentative estimation that as many as 4% of stars may have very wide (>200 AU) high-mass planets or very low-mass brown dwarfs (Ireland et al. 2011). Sco-Cen has also been a favourable target region for multiplicity studies (e.g. Shatsky & Tokovinin 2002; Kouwenhoven et al. 2007). Some of the reasons for this are the uniformity of the region in distance and age, and the high completeness that can be reached down to low companion masses.

It is well known that multiplicity properties depend on the mass of the primary star (e.g. Duchêne & Kraus 2013), and extensive multiplicity surveys have been performed over several different mass ranges in recent years (e.g. Kouwenhoven et al. 2007; Raghavan et al. 2010; Janson et al. 2012a). However, intermediate-mass stars in the range of ~ 1 – $3 M_{\text{sun}}$ has received relatively little attention in this regard. Hence, it is an interesting range for testing the consistency and

*Based on Gemini observations from programs GS-2011A-Q-44, GS-2012A-Q-18, GS-2012A-DD-6, GS-2013A-Q-21, and on ESO observations from program 089.C-0422(A).

¹Department of Astrophysical Sciences, Princeton University, Princeton, NJ, USA; janson@astro.princeton.edu

²Department of Physics, University of Montreal, Montreal, QC, Canada

³Department of Astronomy and Astrophysics, University of Toronto, Toronto, ON, Canada

⁴Osservatorio Astronomico di Padova - INAF, Padova, Italy

⁵European Southern Observatory, Santiago, Chile

⁶Department of Astronomy, Stockholm University, Stockholm, Sweden

⁷Department of Physics and Astronomy, University of Delaware, Newark, DE, USA

⁸Hubble fellow

continuity of dependencies in multiplicity properties on stellar mass. It is also an interesting mass range from the point of view of exoplanet imaging, since several planets and low-mass substellar companions have been imaged around such primaries (Marois et al. 2008; Lagrange et al. 2009; Carson et al. 2012), which has motivated targeted surveys of intermediate-mass stars in the recent past (Janson et al. 2011; Vigan et al. 2012).

Motivated by these issues, we have performed a snapshot imaging survey of 138 Sco-Cen stars with spectral types primarily in the F-type and late A-type range that have not been previously observed in a high-contrast context, to assess stellar multiplicity with a high completeness down through the brown dwarf range, and sensitivity to planetary masses at wide separations. The survey is performed in the context of other studies of multiplicity in young stellar associations that we are performing or have recently performed, including one survey in Chameleon I (Lafrenière et al. 2008b), one in the Taurus star-forming region (Daemgen et al., in prep.), and one specifically in USco (Lafrenière et al., in prep.). Together, these surveys will span an age range of ~ 1 –10 Myr.

The paper is structured in the following way: In Sect. 2, we describe the observational aspects of the study, with a description of the sample in Sect. 2.1, the observational setup in Sect. 2.2, and the data reduction procedure in Sect. 2.3. The results and their analysis are then presented in Sect. 3, including the astrometric analysis in Sect. 3.1, the determination of companion properties in Sect. 3.2, the completeness estimation in Sect. 3.3, statistical properties in Sect. 3.4 and individual notes for particular targets in Sect. 3.5. Finally, we discuss our results in a broader context in Sect. 4.

2. Observations and Data Reduction

2.1. Sample Selection

Our sample consists of early-type stars in the Sco-Cen region. It was selected among all targets identified as Sco-Cen members in (de Zeeuw et al. 1999) that fulfilled two criteria: 1) They had to have a measured parallax and proper motion by Hipparcos, and 2) they had to have been previously unobserved with adaptive optics (AO) instruments on large telescopes; i.e., in the surveys of Shatsky & Tokovinin (2002) or Kouwenhoven et al. (2007), or in our NIRI survey of the USco region (Lafrenière et al., in prep.). The Hipparcos-based requirement allowed for auto-

matic selection of targets with well-determined kinematics and distances, which is important both for a high fidelity in selection of bona fide members, as well as being helpful for the physical interpretation of any discovered companions. Indeed, the vast majority of early-type Sco-Cen stars that were followed up in Chen et al. (2011) were confirmed as real members, whereas later-type stars had a lower confirmation rate. Likewise, all our targets that have been studied in Rizzuto et al. (2011) were assigned high membership probabilities. The visual brightness limit of Hipparcos of $V \sim 9$ mag also matches well with the range of optimal performance for AO wave front sensors, and thus ensures that a good contrast can be achieved in each case (provided acceptable ambient conditions). The avoidance of Shatsky & Tokovinin (2002) and Kouwenhoven et al. (2007) targets helped both to ensure a maximal utility of our survey in terms of mapping the full multiplicity properties of Sco-Cen, and also honed in on an interesting range in planet properties – since the previous surveys focused largely on more massive stars (B- and early A-type), the remaining targets are primarily F- and late A-type (with a few cases of early G-type), which is a range that has not been covered as extensively in multiplicity studies as most other spectral type ranges thus far.

As a result of these selections, our total sample consisted of 145 stars of which 138 were eventually observed, which have a median mass of $1.5 M_{\text{sun}}$ and range from $1.0 M_{\text{sun}}$ to $4.2 M_{\text{sun}}$ (mass determinations are described in Sect. 3.2). While 4 stars have masses of $>5 M_{\text{sun}}$, they were imaged with a different instrumental setting that disfavors a homogenous analysis, and by chance several of them were also taken under rather poor conditions, hence they have simply been excluded from any statistical analysis. The ages of the targets adopted for the analysis performed here are 5 Myr for the (relatively few) USco members and 10 Myr for the UCL and LCC members. These ages have been under discussion in the recent literature, with Pecaute et al. (2012) suggesting an older age, but we base our estimates on the Song et al. (2012) analysis, which empirically demonstrates UCL and LCC to be younger than β Pic, adopting an age of 10 Myr in both cases. The USco region is not discussed in Song et al. (2012), but since it is known to be younger than UCL and LCC, we adopt the original age of 5 Myr (de Zeeuw et al. 1999). There are two scientific issues studied here that are in principle impacted by the age: The detection limit estimation, and the mass ratio de-

terminations. However, as we will discuss in the individual sections, the impact of a factor ~ 2 change in age would be modest for the purposes of this study. The targets are summarized in table 1.

2.2. Observational Procedure

The first epoch imaging was performed in the Spring of 2011, using the NICI AO-assisted camera (Artigau et al. 2008) at the Gemini South telescope in Chile. Out of 145 proposed targets, 115 were observed during this period. Follow-up of 53 targets with companion candidates was executed with the same instrument one year later, during observing cycle 2012A. Furthermore, due to an unforeseen excess in available observing time with NICI, our 2011A program was re-introduced into the queue in 2012A, and an additional 23 targets were imaged, for a total of 138 targets observed in at least one epoch. Some candidates that had indications of sharing a common proper motion with the primary were followed up spectroscopically, either using VLT/NACO (Lenzen et al. 2003; Rousset et al. 2003) during ESO period 89 for simultaneous H+K coverage with AO-assisted slit spectroscopy, or using Gemini/NIFS (McGregor et al. 2002) during 2012A for AO-assisted H-band integral field spectroscopy. Some targets were also followed up in a third astrometric epoch using excess time for the 2012A program that arose from efficient scheduling and execution of the observations. Finally, in period 2013A we performed follow-up of those targets with candidates that had only been observed in one epoch during 2012A, in addition to acquiring another epoch of imaging for the particularly puzzling targets HIP 80130 and HIP 82569.

Our imaging observations were optimized for a high observing efficiency, and consisted of two sequential exposures per target, where the first exposure included 10 coadds of 0.38 seconds each, which is the minimal individual integration time available for NICI. The second exposure consisted of a single 80 second integration. The dual band imaging mode was employed with the 50/50 beamsplitter, using the K_s filter in the red channel and the $H_2(1-0)$ filter in the blue channel. The $H_2(1-0)$ filter is a narrow-band filter within the K -band range, with almost identical pivotal wavelength ($2.12 \mu\text{m}$) to the K_s filter. In this way, we achieved a nearly simultaneous and very wide dynamic range, with the primary star being generally non-saturated in the short $H_2(1-0)$ exposures, and with good sensitivity with respect to the read noise limit for

faint candidates in the long K_s exposures. Each target was subjected to a random offset of $< 5''$ after acquisition. This allowed adjacently observed targets to be used as sky frames for each other, in the same way as during dithering/jittering, but applied on a sequence of targets instead of a sequence of images of a single target. The observations were generally acquired under average to good conditions (fulfilling the Gemini 70 percentile image quality condition), with a few exceptions that are marked in Table 1 and excluded from any statistical analysis.

The spectroscopic observations were mainly utilized for the analysis presented in (Janson et al. 2012b), but were also useful for some of the targets presented specifically here. Summarizing the description in the previous work, the NACO spectra were taken in the $H + K$ setting with a spectral resolution of $R \sim 550$ and a simultaneous coverage from 1.33 to $2.53 \mu\text{m}$. An ABBA nodding along the 172 mas wide slit was employed for background subtraction, with a nod throw of $10''$. One initial AB cycle was taken with short integration times of 1 s and 12 coadds, followed by a series of 100 s exposures, structured as 3 AB cycles with 5 s by 20 coadds for the brightest candidates and 10 AB cycles with 25 s by 4 coadds for the faintest. The short exposures allow for the primary to remain non-saturated such that it can be used as a reference star, and the long exposures minimize the read noise allowing for a high S/N of the companion candidate. The NIFS spectra were taken in H -band with a spectral resolution of $R \sim 5000$ covering a spectral range of 1.49 to $1.80 \mu\text{m}$. Each sequence observation started with a dither sequence with 21 s integration times with the central star in the field of view, to get non-saturated spectra of the primary for the purpose of using it as a standard star. This was then followed by a deeper dithering sequence with integration times of 240 s, with the companion candidate included in the field of view. If the separation of the candidate was small enough that the NIFS field of view ($3''$ on each side) could fit both the star and companion then this was accommodated, otherwise the field was centered on the candidate.

2.3. Data Reduction

Data reduction for the NICI imaging was performed using custom IDL routines, since the observational strategy was somewhat novel and thus required flexibility in the reduction procedure. For each image file, the red and blue channel images were extracted and an-

alyzed separately. As a first step, flat fielding and bad pixel removal were applied, followed by a background subtraction, in which a median of several adjacent images were taken and subtracted from each individual image. Distortion correction was applied using the separate distortion solutions for the red and blue channel provided on the NICI homepage¹, with a quadratic interpolation scheme. By default, North points downward in NICI images, and the red and blue channels are mirror images of each other, with one having a right-handed and the other a left-handed orientation. Which channel is oriented which way depends on whether NICI is mounted in an up-looking or side-looking configuration. Thus, since the instrument was mounted in different configurations at different epochs, the orientation switched between the red and blue channels between images. All images were re-oriented into a common framework with North pointing up and East to the right, taking these various circumstances into account. Finally, the images were shifted using spline interpolation, such that the primary star became centered on the central pixel. For this purpose, Gaussian centroiding was used for the $H_2(1-0)$ images, where the star is unsaturated in the short exposures. For the K_s images, where the primary is typically saturated even in the short exposures, manual centering by eye was applied. As described in Janson et al. (2012b), this gives a smaller scatter in the background star astrometry than a range of other methods tested for the purpose, and the good consistency between the independent $H_2(1-0)$ and K_s astrometry noted in Sect. 3.1 further demonstrates the validity of the method.

In the same way as for the NICI imaging, the NACO spectroscopy data reduction was also performed with a custom IDL pipeline, since we had a set of routines available from a previous observing program (Janson et al. 2010) which could be easily adapted to form part of the pipeline. The procedure started with flat fielding and bad pixel removal. Each AB set was then pairwise subtracted to remove the background. The spectral traces are (nearly) vertical on the NACO detector, hence for each pixel row, the photocenter of the star was determined through Gaussian centroiding. This works well not only for the non-saturated sequences, but also for the longer-exposure sequences, since the stars are only mildly saturated. A spectral trace was then fitted to the centers of the respective rows, and all data were shifted so as to form a perfectly

vertical spectral trace, with the photocenter of the star at the central pixel column, for all frames in each observational sequence. One collapsed frame of the collected non-saturated data and one of the saturated data were produced using a regular mean combination. At this point, the secondary spectra were clearly visible at their known positions in the deep exposures, and could be extracted using an interpolation between the fluxes measured directly inside and outside of the location of the secondary as an estimation of the stellar PSF at that location. A 162 mas aperture was used in the extraction of both the stellar and companion spectra. Wavelength calibration was performed using a combination of telluric features and intrinsic features in the stellar spectra. For flux calibration, the primary star was modeled as a single-temperature blackbody. The extracted companion spectrum was divided by the fraction of the stellar spectrum to the model blackbody, which eliminates all telluric features from the companion's spectrum. Intrinsic stellar features remain as contaminants, but as noted in Janson et al. (2012b), such features are rare and weak in these early-type stars, and do not affect the largely continuum-based analysis that they are used for.

Basic data reduction of the NIFS data was done using the facility-provided IRAF pipeline. This executed all fundamental steps such as flat field correction, distortion correction, wavelength calibration, and data cube construction. The final steps of registering and shifting all frames to a common center, as well as extracting the spectra, were done in IDL. Each wavelength slice of each data cube was treated as an individual image, being centroided and interpolated in the same way as described for the imaging above. Extraction was performed using a 172 mas circular aperture.

3. Analysis and Results

In this section, we describe the various analyses that were applied to the companion candidates detected in the images, and their results. The candidates considered for analysis here are exclusively those that have a projected separation between $0.1''$ and $5.0''$ from their parent stars. There are two reasons for the outer limit: Firstly, while the NICI field of view is $18''$ on each side, the dithering scheme with different stars being placed at different parts of the detector means that the completeness drops rapidly outside of $5''$. Secondly, the false positive rate scales with the square of the angular separation, such that essentially all targets have

¹<http://www.gemini.edu/?q=node/10493>

false positives at $>5''$, and so follow-up of such very wide candidates becomes observationally inefficient. In total, we have discovered 145 candidates around 79 stars. Of these, 116 are considered either indicated or confirmed background sources, and 29 are considered indicated or confirmed companions (residing in 27 systems, since two systems are triple, see Fig. 1 and Sect. 3.5). To the best of our knowledge, none of the companions have been previously reported in the literature. In addition, there are three cases (HIP 63692, HIP 66001, and HIP 79097) where the PSF of the primary star is extended, which might point to the existence of a partially resolved close companion well inside of $0.1''$, and there are two cases (HIP 50847 and HIP 64322) in which a probable binary companion is seen but the images are among those that were taken in too poor conditions for any solid conclusion to be drawn. These individual cases are discussed in Sect. 3.5.

One of the grounds for assessment of companionship was based on calculated false alarm probabilities of individual candidates. These were estimated in the same way as in Lafrenière et al. (2008b), on the basis of the brightness of the candidate, its separation from the primary star, and the background stellar surface density at its location in the sky. The latter was acquired from 2MASS (Skrutskie et al. 2006) point source counts within a $15'$ radius from the primary star. For a given candidate, we then calculated the number of stars at least as bright as the candidate, which would fall within a circular area out to the separation of the candidate. In this way, a candidate whose properties are reproduced by, e.g., 0.01 background contaminants can be said to have a 1% false alarm probability. It is important to interpret such a number within the context of the full survey – i.e., a 1% probability may seem small, but in a survey such as this one with >100 targets, an occurrence of one such contaminant is entirely plausible.

3.1. Astrometry of Companions and Candidates

As a general broad classification, the candidate companions can be divided into a bright group and a faint group. The brighter candidates generally have very small background contamination probabilities ($\ll 1\%$), favourably small separations, estimated masses in the stellar regime, and are visible in both the K_s and the $H_2(1-0)$ images. The fainter candidates, by contrast, generally have high contamination probabilities ($\gg 1\%$), favourably large separations, es-

timated masses in the planetary regime if they would be interpreted as companions ($\sim 5\text{--}15 M_{\text{jup}}$), and are generally not visible in the $H_2(1-0)$ images. There are a few intermediate cases, some of which were discussed in Janson et al. (2012b) and the rest of which will be discussed individually here, but first we will discuss the separate analyses that were applied to the two distinct populations.

The brighter candidates, as mentioned, were visible in both K_s and $H_2(1-0)$ images, and so astrometric analysis was performed independently in the two channels for these candidates. We used Gaussian centroiding for determining the positions of the companions in both cases. The astrometry was found to be well consistent between the two bands, except for a systematic rotational shift of 1.17° in the $H_2(1-0)$ data with respect to the K_s data, which switches sign between the up-looking and side-looking instrumental configurations. Hence, we interpret the blue channel as having a 1.17° rotational offset that is corrected for by de-rotating the images by the corresponding amount. We then evaluate errors in the astrometry on the basis of the scatter between the $H_2(1-0)$ and the K_s astrometry. We do this separately for the very close ($\leq 0.5''$) and the wider ($0.5''\text{--}5''$) population of candidates, and find errors of 4 mas in separation and 0.9° in position angle in the former case, and 8 mas and 0.4° respectively in the latter.

Given that these objects have very low contamination probabilities and increase in frequency toward smaller angular separations in an opposite way from what would be expected for background stars, they are considered to be probable companions and are considered as such for the remainder of the discussion. They have not been confirmed with common proper motion, except in cases where a fainter candidate was followed up in the same system. Among the targets that were followed up for this reason, HIP 58220 B can be confirmed as a common proper motion companion. HIP 57595 B could not be accurately registered in the second epoch due to overlap with a bright side-lobe from the primary star, although by eye it does appear to share a common proper motion. HIP 75891 B and HIP 77520 B are consistent with common proper motion, but the background hypothesis cannot be rejected due to a small motion of the primary stars relative to the astrometric precision. One exception, however, is HIP 72630, where the candidate has a false alarm probability of only 0.3%, but the proper motion analysis nonetheless shows that it is a background con-

taminant. The candidate has the highest false alarm probability of all the targets with $\ll 1\%$, hence while its presence is relatively unlikely, it is not particularly surprising. It does however demonstrate that common proper motion testing would be an important aspect of providing final proof of companionship for the individual binaries, and to weed out any potential contaminant that could conceivably remain in the sample, e.g. HIP 58528 B (false alarm probability of 0.2%) or HIP 67428 (0.3%).

The fainter candidates are generally not visible in the $H_2(1-0)$ images, but as noted above, the astrometry in K_s and $H_2(1-0)$ are well consistent, hence we proceed with astrometry on K_s alone for this population. It is known a priori that the vast majority of these candidates must be background contaminants from the calculated probabilities alone, so CPM (Common Proper Motion) analysis is certainly necessary in order to detect any real companions among them. Thus, all of the faint candidates have been followed up in at least one additional epoch. Since Sco-Cen targets move rather slowly on the sky, the confidence level of the common proper motion testing rarely reaches 3σ or higher. However, the candidates move by a median amount of 27 mas, larger than the residual scatter of 13 mas, and the median difference between the candidate motion and the expected background trajectories is only 4 mas. Hence, the typical faint candidate shows a motion that is well consistent with background motion, and is distinct from common proper motion by just above the 2σ level.

Nonetheless, at these levels of confidence, both real companions and background contaminants can plausibly exist among the candidates that experience relatively little motion. Hence, for the target that seemed to move the least or sometimes not at all, we performed further follow-up in a third epoch of astrometry, as well as with spectroscopy in many cases. In this way, the brown dwarfs discussed in Janson et al. (2012b) were confirmed as companions (HIP 65423 B, HIP 65517 B, and HIP 72099 B), both through the CPM and spectral analyses consistently. Similarly, most of the rest of the targets could be confirmed as background contaminants in the CPM analysis, and in the cases where spectra were acquired (e.g. for the candidates around HIP 62677 and HIP 72584) a consistent result was acquired. However, there are two cases that remain puzzling in this regard. These targets – HIP 80130 and HIP 82569 – will be discussed in more detail in Sect. 3.5. The multi-epoch astrometry

is summarized in Table 2.

3.2. Companion Properties

In order to determine the physical properties of the binaries discovered in our sample, we first calculate their photometric properties. The secondaries in the systems are typically clearly visible and non-saturated in both the short $H_2(1-0)$ and the short K_s exposures. The primaries, on the other hand, are typically only non-saturated in the $H_2(1-0)$ filter. However, the pivotal wavelengths of the respective filters are almost identical ($2.12 \mu\text{m}$ in both cases), which means that the $[H_2 - K_s]$ color is essentially independent of stellar temperature. Indeed, integration of the flux in the bandpasses of the respective filters shows that the difference in this color between a 5000 K and a 10000 K blackbody is less than 0.01 mag. This temperature range encompasses all of our primary stars as well as Vega, implying that in Vega magnitudes, the $H_2(1-0)$ and K_s magnitudes are essentially identical. As a result, we can estimate the primary flux count in the K_s image by multiplying the measured count in the $H_2(1-0)$ image with a uniform factor. We determine this factor by measuring the fluxes of all secondaries that are non-saturated in both images, and find that the number is 14.02. Hence, we can estimate the K_s -band binary flux ratios by estimating the primary counts in this way and by measuring the secondary counts directly. In addition, we can measure the $H_2(1-0)$ -band binary flux ratios directly in the image, and by comparing the ratios we can cross-validate the method, and get an estimate of the errors associated with it. We find that the two measures are consistent to within 0.2 mag, which we use as the photometric error. In all cases, we use a circular aperture of 72 mas diameter to determine the counts.

For calculating masses of the various components, apparent K -band magnitudes are adopted from 2MASS (Skrutskie et al. 2006), and the primary and secondary magnitudes are calculated using the flux ratios described above. The apparent magnitudes are translated into absolute magnitudes using distance moduli based on the Hipparcos parallaxes (Perryman et al. 1997). This is then used in conjunction with isochrones at the ages of the Sco-Cen sub-groups to derive masses. In our case, we use the Siess et al. (2000) isochrones, since they cover the full range of stellar masses in our sample from $0.1 M_{\text{sun}}$ to $5 M_{\text{sun}}$. However, we also compare the results to the Baraffe et al. (1998) isochrones in the overlapping

range of $\leq 1.4 M_{\text{sun}}$ and find that at these ages and masses, the predicted K -band magnitudes are consistent to within 0.1 mag between the models, which is smaller than the photometric error. We also use the Baraffe et al. (1998) isochrones for one secondary with a mass of $< 100 M_{\text{jup}}$, i.e. outside of the range of the Siess et al. (2000) models. The magnitudes and masses of the binary components are listed in Table 3.

3.3. Detection Limits

For evaluating the detectability of companions around any given star in the survey, and for evaluating the completeness to such companions in the survey as a whole, we must first calculate contrast curves. This is done in a very similar manner to the contrast calculation of actual binaries described in Sect. 3.2, by estimating the primary flux count in the deep K_s -band images from the non-saturated $H_2(1-0)$ count and factoring in the filter translation, as well as the difference in integration times. The standard deviation is calculated in a series of annuli at different separations from the central star to acquire σ as a function of angular separation, and a 5σ criterion is used as the detection threshold. Normalizing the 5σ curves by the primary flux gives the contrast curve, and factoring in the primary magnitude and the distance modulus as in Sect. 3.2 gives the detectable absolute magnitude as function of separation around each star. Since these limits correspond to planet and brown dwarf masses, we use DUSTY (Chabrier et al. 2000) models for temperatures of > 1700 K and COND (Allard et al. 2001; Baraffe et al. 2003) models for < 1700 K for translating magnitude limits into mass limits, given the estimated ages. The completeness of the survey as a whole can then be calculated as a 2D function of separation and mass by evaluating what fraction of the targets provide detectability for companions of any given mass and separation. We plot some contours of this function in Fig. 2. There are bumps in the individual contours due to strong PSF sidelobes and similar features in the images. As an example, we find that the completeness is 70% for $10 M_{\text{jup}}$ planets outside of $1.2''$, which corresponds to 160 AU at the median distance of the sample of 132 pc.

The detection limits quoted in terms of mass depend on the exact ages of the systems, hence given the uncertainty in age of the Sco-Cen association as discussed above, they should be treated with a certain degree of caution. However, the impact of the factor ~ 2 uncertainty in age has a modest impact for the masses

near our detection limits. For instance, according to the DUSTY models (Chabrier et al. 2000), a $10 M_{\text{jup}}$ object at 5 Myr has the same K-band brightness as a $\sim 13 M_{\text{jup}}$ object at 10 Myr. Our 70% completeness limit quoted above would thus only increase by $\sim 30\%$ if the Pecaute et al. (2012) ages were applied.

3.4. Statistical Properties

Here we will consider the statistical distributions of the binary population in our observed sample. Fig. 3 displays the projected separation versus the mass fraction of the detected binaries. The most striking trend is a lack of nearly equal-mass binaries, particularly at large separations. This cannot be caused by any bias related to our detection limits, both because the completeness is very good over our whole considered separation range of $0.1''$ to $5.0''$ for masses down to our lowest-mass detected companions of $\sim 50 M_{\text{jup}}$ as shown in Sect. 3.3, and also because our sensitivity increases outward in separation and upward in mass, and is maximal in the range where the lack of companions is observed. The inferred masses of the individual components depend on the age, but since both components evolve with time, the impact of age uncertainties of the relevant order is limited on their calculated mass ratio. For instance, according to the Baraffe et al. (1998) models, a $1 M_{\text{sun}}$ primary and $0.1 M_{\text{sun}}$ secondary at 10 Myr (the approximate UCL/LCC age according to Song et al. (2012)) correspond in K-band brightness to a $1.1 M_{\text{sun}}$ primary and $0.13 M_{\text{sun}}$ secondary at 16 Myr (the corresponding Pecaute et al. (2012) age). Hence, the mass ratio only changes from 0.10 to 0.12 between the younger and older age, and the impact decreases as the mass ratio gets larger, since the evolution of the components becomes more equal. As a result, the age uncertainty has a small impact on the observed mass ratio distribution, and cannot explain the lack of near equal-mass binaries.

We can attempt to quantify the companion mass ratio distribution with a simple power law, $f \sim q^{\alpha_q}$, where f is the frequency, q is the mass ratio (secondary to primary, i.e. between 0 and 1), and α_q the power law index. This is done by generating simulated populations with a given distribution determined by α_q and comparing to the observed population using a Kolmogorov-Smirnov test. For each population we generate 1000 binaries, and 1000 populations are being simulated in order to verify the robustness of the results. Cases where the secondary mass is

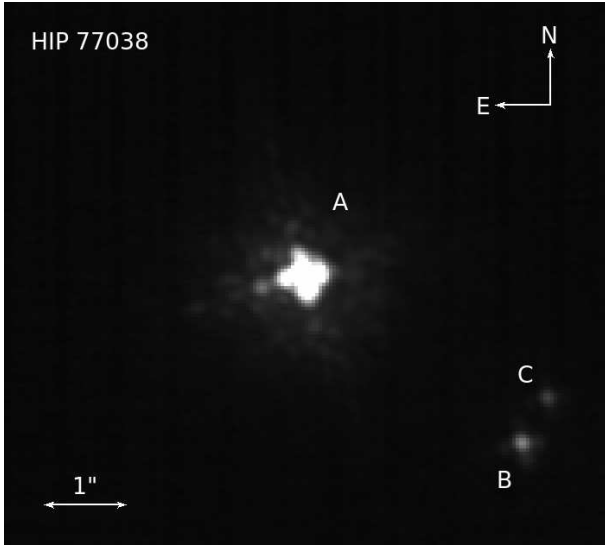


Fig. 1.— Example image from the survey, showing the triple system HIP 77038. The tertiary component is a very low-mass star, with an estimated mass of $\sim 90 M_{\text{jup}}$. The apparent point source to the East of the primary at a small separation is a known ghost feature.

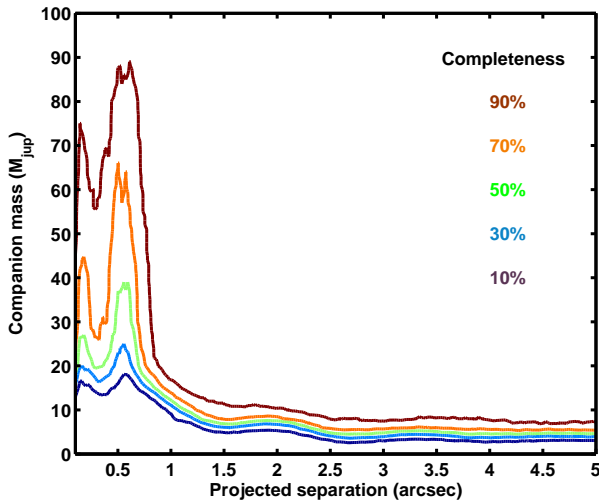


Fig. 2.— Countours of the survey completeness as a function of separation and companion mass. The observations are essentially fully complete to stellar companions within $0.1''$ – $5.0''$, and provide good completeness down to planetary masses at wide separations.

$< 50 M_{\text{jup}}$ are removed in order to maintain a good completeness, hence the power law fit is only valid down to secondaries of this mass. The full range of separations (0.1 – $5.0''$) is included in the comparison. The median probability among the 1000 simulations is adopted as the result of the full test, and the 5th and 95th percentiles are taken as the lower and upper bounds, respectively. This is equivalent to the procedure applied in Babu & Feigelson (2006). In this way, we can firmly exclude that the mass ratio is uniformly distributed, since simulated populations with $\alpha_q = 0$ have a $1.4 \times 10^{-7} \pm 0.4 \times 10^{-7}$ probability of matching the observed distribution. It is necessary to make α_q substantially negative (bottom-heavy mass ratio distribution) to get better fits. A value of $\alpha_q = -0.4$ which has been used for more massive stars (e.g. Kouwenhoven et al. 2007) is still too shallow, with a probability of $0.023^{+0.007}_{-0.005}\%$. $\alpha_q = -0.9$ fits better at $17.5^{+0.04}_{-0.03}\%$. However, this form of power law fitting does not have a promising asymptotic behaviour, as it starts to drastically overshoot at small mass ratios for steep power law indices. Hence, we slightly alter the form of the distribution, and formulate it as $f \sim 1 - q^{\beta_q}$, which better fits the observations for a range of values of β_q . Note that in this framework, a higher β_q implies a more bottom-heavy mass ratio distribution, i.e. in the opposite sense to α_q . Stepping through β_q in steps of 0.5, we find that the best fit is provided by $\beta_q = 2.5$, which has a $66.6^{+4.1}_{-3.8}\%$ probability of matching the observed distribution, hence we adopt this value for the remainder of this analysis.

The semi-major axis distribution is another issue of interest to address. We do this in a very similar way as above, simulating populations with given distributions and comparing them to the observed distribution using a Kolmogorov-Smirnov test. For translating from our observed projected separations into semi-major axes, we multiply the separations by a factor 1.02. This was calculated based on Brandeker et al. (2006) as the conversion factor between semi-major axis and projected separation for a sample with an assumed eccentricity distribution of $f(e) \sim 2e$. For a less eccentric distribution, the conversion factor can be somewhat higher, up to a maximum of 1.27 for completely circular orbits. For instance, Fischer & Marcy (1992) calculate a factor 1.26 for their M-dwarf sample. We have tried the same analysis as below with a 1.26 conversion factor, and found that it makes very little difference for the results and has no impact on the conclusions. Hence, in the procedure described in the following, only the

factor 1.02 is used.

Relative to the mass ratio case, a comparison of the semi-major axis distribution to other distributions in the literature is less discriminating, partly due to the fact that the binaries here cover a somewhat limited semimajor axis range relative to the extremely wide range that occurs in the universe, spanning approximately six orders of magnitude from a few Solar radii to tens of thousands of AU. For Sun-like stars, a log-normal distribution with $\mu_a = 1.64$ and $\sigma_a = 1.52$ has been measured (Raghavan et al. 2010). Applying this relation in our simulations results in a $29.9^{+4.5}_{-3.9}\%$ probability that it is drawn from the same distribution as our observed sample. For more massive stars, it has been suggested that Öpik’s law (Öpik 1924) might provide a better fit than a log-normal distribution (Kouwenhoven et al. 2007). Öpik’s law represents a uniform distribution in logarithmic semi-major axis space. In this sense, it can be seen as a log-normal distribution with infinite σ_a . Applied to our sample, Öpik’s law results in a $39.3^{+5.6}_{-5.4}\%$ matching probability. Thus, while neither of these distributions fit extremely well, neither can be more than at best marginally excluded. This is consistent with a picture in which intermediate-mass objects have an intermediate distribution between lower-mass and higher-mass stars. We note that if we adopt a log-normal distribution and simply shift the Sun-like distribution to wider separations, $\mu_a = 2.40$ and $\sigma_a = 1.52$, we get a $67.2 \pm 5.1\%$ probability match, hence we adopt this relation for future purposes. In all of these cases, we set lower and upper bounds on the semi-major axis of 0.023 AU and 23000 AU, respectively (Kouwenhoven et al. 2007).

The multiplicity fraction within $0.1'' < \rho < 5.0''$ is $27/130 = 20.8\%$, with 4.0% errors assuming Poissonian statistics. If we were to assume a total multiplicity fraction of 100%, then adopting the best-fit distributions in mass ratio and semi-major axis as above, and accounting for the completeness function, would result in a higher multiplicity fraction within $0.1'' < \rho < 5.0''$ of 35.1%. Hence, these distributions imply that the actual total multiplicity should be approximately 59%, in order to reproduce the 20.8% multiplicity observed in our covered observational range. Obviously, there is significant uncertainty in this number, primarily due to the limited coverage in semi-major axis space. For instance, if we were to adopt Öpik’s law instead, then the total implied multiplicity fraction would be 81%. However, since the distribution is as narrow as the Sun-

like distribution in the former case, and it cannot possibly be broader than the Öpik distribution adopted in the latter case, it is probably fair to conclude that the total multiplicity fraction is bounded between 59% and 81% for any realistic distribution.

3.5. Individual Notes

Here we provide individual notes for targets for which special information exists.

HIP 50083: HIP 50083 is one of the four stars that have a mass of $>5 M_{\text{sun}}$, and is therefore excluded from the statistical study. The image is of insufficient quality to put any stringent constraints on the presence or absence of companions.

HIP 50847: The image of HIP 50847 is of too poor quality to be scientifically useful. Nonetheless, there is a probable bright binary companion visible in the image, at a separation of $\sim 2.2''$ and a position angle of $\sim 351^\circ$. HIP 50847 is one of the four $>5 M_{\text{sun}}$ stars that were omitted from any statistical analysis. Aside from the possible companion reported here, HIP 50847 (HD 90246) is a known double-lined spectroscopic binary with a period of ~ 15 days (Quiroga et al. 2010), hence the system is possibly triple.

HIP 56543: There is a bright source at the edge of the field, at a separation of $9.92''$ and a position angle of 310.7° . Thanks to the large separation and relatively small brightness contrast, this source is visible in 2MASS (Skrutskie et al. 2006) with designation 2MASS J11353717-5043180, at a separation of $10.24''$ and position angle of 309.3° from HIP 56543. The expected motion of HIP 56543 relative to a static background object over the ~ 12 year baseline is 343 mas West and 31 mas South, fully in agreement with the observations. Hence, we can conclude that 2MASS J11353717-5043180 is a background star, physically unrelated to HIP 56543.

HIP 57238: While the PSF of HIP 57238 is extended, it is extended to the same degree and in the same direction in both the primary and the well-resolved secondary in the system. Hence, we conclude that it is likely to be a PSF artefact.

HIP 58899: This is one of the two systems in the sample that are triple within the sensitivity range of the survey. For the statistical investigations of mass ratio and semi-major axis, HIP 58899 is counted as two pairs, where the tight AC pair is counted as a regular pair, and the wider AB pair is counted as another pair but the A+C mass is used for the A component.

HIP 59481: Given its relatively low contamination probability of 1.1%, and the fact that it was the only point source in the field of view, the candidate companion to HIP 59481 was considered one of the most interesting targets for follow-up after the first epoch of imaging. However, the astrometric follow-up clearly shows that it is a background contaminant.

HIP 63962: Given a rather extended PSF, HIP 63962 may be an unresolved binary, with a separation of a few tens of mas (well under 50 mas) and a position angle of $\sim 40^\circ$.

HIP 64322: This star was observed under too poor conditions for the images to be scientifically useful, but a probable bright binary companion is visible at a separation of $\sim 2.3''$ and a position angle of $\sim 170^\circ$. Like all images of insufficient quality, it is omitted from the statistical analysis.

HIP 66001: Since the PSF of HIP 66001 is extended, it may be an unresolved binary. The separation would be a few tens of mas (well under 50 mas), and the position angle $\sim 30^\circ$.

HIP 77038: HIP 77038 is one out of the two systems in the survey that are triple systems. For statistical purposes, when counting mass ratio and semi-major axis, the system is counted as one pair in which the primary is one component, and the sum of the tight BC pair is the other component. The BC pair itself is not counted as a pair in this context, since the components are both late-type, and thus the mass of B is outside of the range of interest in primary mass.

HIP 78384: Also known as η Lup, this is one of the four $> 5 M_{\text{sun}}$ stars that are excluded from our statistical study. The system is known as a probable triple system (e.g. Eggleton & Tokovinin 2008), but both the secondary and tertiary components are outside of the NICI field of view.

HIP 79097: Apart from the clearly resolved companion at $0.8''$ separation, there is an additional extension in the HIP 79097 A component, which is not present in the companion. This strongly implies that a third component is present in the system as a close companion to component A, with a separation of a few tens of mas (well under 50 mas) and a position angle of $\sim 110^\circ$.

HIP 79977: This star has a debris disk that was recently spatially resolved (Thalmann et al. 2013). The deep image in Thalmann et al. (2013) also has two faint point sources within $5''$. Our image is too shallow to detect either the disk or the point sources at a statis-

tically significant level, although the point sources can be traced at their expected background positions with prior knowledge of where to look.

HIP 80130: The most puzzling target in the survey, HIP 80130 has a faint point source residing at $4.1''$ separation from the star, which was identified as a candidate very low-mass brown dwarf in the first epoch image, and thus was followed up in a second epoch. The second epoch showed indications of common proper motion, so it was followed up in third (and subsequently a fourth) epoch of astrometry, and with spectroscopy. The photometry over the four epochs suggests strong variability, with $\Delta K = 7.1 \pm 0.8$ mag. The astrometry in all four epochs, spanning approximately two years, is essentially perfectly consistent with common proper motion, and is inconsistent with the expected background trajectory by a total of 10.0σ (see Fig. 4). On the other hand, the spectrum of the candidate favours a different interpretation. The best-fit spectral type is in the range of $\sim M3$ (see Fig. 5), implying a temperature of 3300 K (Slesnick et al. 2004). Using the Baraffe et al. (1998) models and an age of 5 Myr, the implied mass is $\sim 250 M_{\text{jup}}$ and the corresponding predicted absolute magnitude is $M_K = 5.25$ mag. This is wildly at conflict with the actual magnitude measured in the image (if we assume that the candidate is indeed comoving with HIP 80130) of $M_K = 8.69$ mag, which by itself yields a mass of $\sim 18 M_{\text{jup}}$ from Chabrier et al. (2000). Thus, there is a discrepancy of 3.44 mag (a factor of 24) in brightness, or equivalently a factor of 14 in mass, between the estimations based on spectral type and apparent brightness, respectively. The gap is too large to be explained by any model uncertainties or errors in (e.g.) distance, or the variability of the source.

A further observational constraint that underlines the peculiar nature of the source comes from the fact that HIP 80130 was covered in the UKIDSS survey (Lawrence et al. 2007) in a K -band image from epoch 2009.34. A point source is reported at a separation of $4.09''$ and a position angle of 111.0° , which corresponds to our identified point source. The location is considerably closer to the CPM location than the background trajectory, lending further support to the CPM hypothesis. The K -band contrast is 6.9 mag, consistent with our NICI contrast. Hence, the UKIDSS data broadly confirm the picture posed by the NICI data, that this is an unusual object in one way or another. The options that come most readily to mind are that the object is either a very unusual form of compan-

ion, or a background star which by chance has equal proper motion with HIP 80130, both of which seem highly unlikely. Perhaps the object is a 3300 K star which is obscured to an extreme degree (for its age), for instance by an edge-on disk. This might be supported by the strong variability. However, given these uncertainties, we cautiously do not include HIP 80130 in any of the statistical analysis for the moment, and we emphasize that more data will be needed to clarify the real properties of the source.

HIP 80208: This is one of the four stars that have a mass of $>5 M_{\text{sun}}$, and is therefore excluded from the statistical study.

HIP 82569: HIP 82569 resides in a crowded field, and has several point sources present within the NICI field of view. Surprisingly, none of the sources appear to move with respect to the primary over four epochs of imaging spanning nearly two years. While the proper motion of HIP 82569 is among the slowest in the sample at 24.4 mas/yr, it should be significant over the 2-year baseline. The normal inference for any single point source would be that it shares a common proper motion, and thus is a companion to the star. However, ~ 10 point sources at similar projected separations, and some of which are evidently binaries themselves, cannot be companions to the same star. Hence, we consider the proper motion of this star to be unreliable and count the point sources as probable background sources. Further analysis in the future will be required to stringently test whether single sources in the field may nonetheless share a common proper motion with HIP 82569.

4. Discussion

The total multiplicity fraction that we derive of $\sim 60\text{--}80\%$ (depending on the semi-major axis distribution) fits very well with the general view that is emerging of a smoothly increasing multiplicity fraction with primary mass. This appears to hold from the brown dwarf range with derived multiplicities of $\sim 10\text{--}30\%$ (e.g. Bouy et al. 2003; Ahmic et al. 2007; Joergens 2008) through M-dwarfs with a multiplicity of $\sim 35\%$ (e.g. Fischer & Marcy 1992; Janson et al. 2012a) and a smooth increase from the lowest to highest M-dwarf masses (Janson et al. 2012a), early K- through late F-stars with $\sim 40\text{--}50\%$ and again a smooth increase from the lower to the higher masses of the range (Raghavan et al. 2010), our sample of F- and late A-type stars with $60\text{--}80\%$, and to more

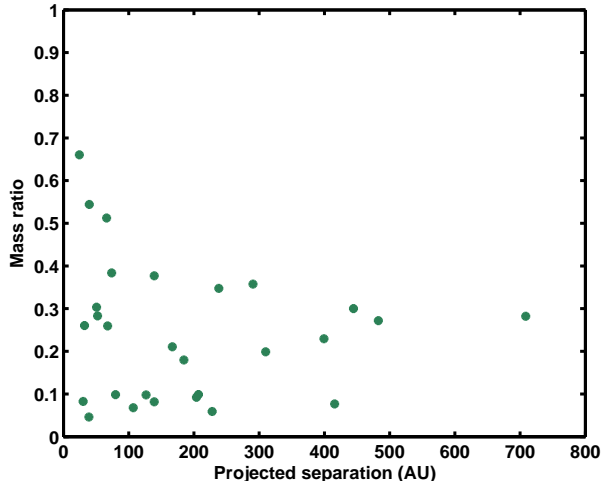


Fig. 3.— Distributions in separation and mass ratio for the binaries in the sample. There is a lack of binaries with components of similar mass, particularly at large separations.

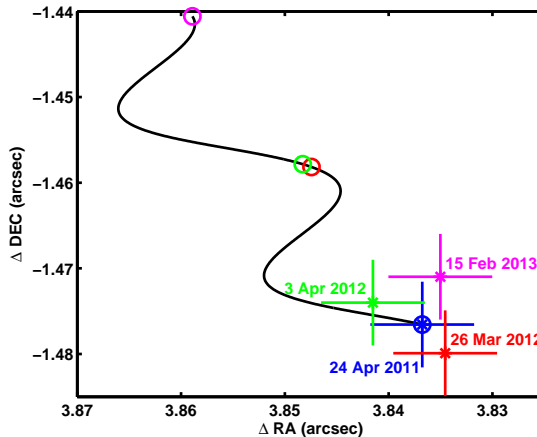


Fig. 4.— Astrometry of the candidate companion to HIP 80130. The static background trajectory can be rejected by 10.0σ in total.

massive A- and B-type stars with $\sim 80\text{--}100\%$ (e.g. Shatsky & Tokovinin 2002; Kouwenhoven et al. 2007) and once again an increase from lower to higher primary masses within the sample (Kouwenhoven et al. 2007). The multiplicity of O-type stars is also consistently very high (e.g. $>80\%$ from SBs alone Chini et al. 2012). Likewise, the semi-major axis distribution appears to fit in with the trend that the characteristic orbital size increases from brown dwarfs (Burgasser et al. 2007) through M-dwarfs (Janson et al. 2012a) and Sun-like stars (Raghavan et al. 2010), since our data implies a further increase of orbital size around AF-type stars. For higher-mass stars, the distribution appears to be best described by Öpik’s law (Kouwenhoven et al. 2007), which is uniform in logarithmic space rather than log-normal, hence the concept of a characteristic semi-major axis is not as well defined. Since our sample is marginally consistent with Öpik’s law, this again fits with the emerging picture that binary properties are universally continuous across all stellar and even brown dwarf properties.

However, one remaining puzzling issue with regards to our sample in particular is the mass ratio distribution. In principle, with the brown dwarf mass ratio distribution being strongly top-heavy and that of low-mass and Sun-like stars being essentially flat (Raghavan et al. 2010; Janson et al. 2012a; see also Goodwin 2013; Reggiani & Meyer 2013), it would be natural to assume that AF-type stars should have a bottom-heavy distribution, as we do observe. However, the distribution is very steep, and significantly more so than what has been found for the higher-mass population (Kouwenhoven et al. 2007), thus breaking the otherwise continuous trend. This effect appears to be physically real, since the most surprising feature of a lack of nearly equal-mass components occurs in the parameter space of maximal detectability. It also seems unlikely that it could be related to any selection bias, although there is, in fact, a selection issue related precisely to massive binary companions discussed in de Zeeuw et al. (1999), which they discuss for (e.g.) the case of USco member δ Sco. This system consists of a massive binary (primary spectral type is B0), unresolved to Hipparcos, where the orbital motion of the binary causes its photocenter motion to deviate from the motion of the center of mass over the relatively short timescales (3.3 years) covered by Hipparcos. In this case, the effect estimated by de Zeeuw et al. (1999) is a 2 mas/yr deviation from the ‘real’ proper motion, larger than the Hipparcos errors

of ~ 1 mas and sufficient to (presumably erroneously) discard it as a USco member based on their standard approach. Hence, other stars with massive companions may have been missed in their procedure, which would in turn potentially cause a selection bias against such targets in our sample. However, it is unlikely that it could be influencing this observational result. The stars in our sample are less massive than δ Sco by an order of magnitude, causing slower orbital motion for a given separation. Furthermore, the separations that we probe stretch out substantially larger than the $0.13''$ separation of δ Sco. As a result, we estimate that the magnitude of deviant motion for $1''$ separation binaries in our sample is an order of magnitude smaller than for δ Sco, which as mentioned above is 2 mas/yr. In this circumstance, they are much smaller than the astrometric errors of ~ 1 mas/yr and cannot influence the kinematic classification of the primary star. Thus, while a selection bias could conceivably be present for small-separation binaries, it cannot affect the range of $>1''$ binaries, where the lack of nearly equal-mass components is the most pronounced. Finally, we note that if such a bias were present, it should have affected the Kouwenhoven et al. (2007) results in the same way, which appears not to be the case as Kouwenhoven et al. (2007) derive a shallower mass ratio distribution. A possible solution can be seen in Fig. 3, where high mass ratios appear to become more common at smaller separations. The three cases of HIP 63962, HIP 66001, and HIP 79097, if interpreted as close binaries, would all have to have two nearly equal-mass components, which would further support this trend. Hence, it is possible that the mass ratio depends on semi-major axis and that our sample would yield a shallower distribution if observed over the full semi-major axis range rather than a quite limited range of it.

As a result of the detections of wide planetary mass objects and low-mass brown dwarfs such as 1RXS J1609 b (Lafrenière et al. 2008a, 2010), GSC 0621 B (Ireland et al. 2011), and HIP 78530 B (Lafrenière et al. 2011), it has been speculated that the Sco-Cen region might have a particularly high frequency of such companions, with Ireland et al. (2011) citing a tentative frequency estimation of $\sim 4\%$ in the 200–500 AU range. If adopting this frequency, then given our high completeness to such companions and the fact that we survey 138 targets of which 130 are of sufficient quality, we should have expected to find ~ 5 companions in the mass range between 1RXS J1609 b and

HIP 78530 B. Given this context, the fact that we find none is quite significant, with a $<1\%$ probability of being consistent with a 4% frequency. A few distinctions between the surveys are worthy of note. Firstly, the surveys in which the above detections were made were performed exclusively in the USco sub-region of Sco-Cen, whereas our survey was performed in the whole Sco-Cen region, with only a small minority of targets being specifically USco members. Thus, in principle there might be something special about USco, although this seems unlikely, since the sub-regions of Sco-Cen are very similar, must have formed under very similar conditions, and vary in age by only a factor of ~ 2 . Secondly, the stellar mass distributions are different between the surveys. However, while 1RXS J1609 b and GSC 0621 B were discovered around Sun-like stars, HIP 78530 B was discovered around a B-type star, so the primary mass range at which detections have been made appear to encompass the range of AF-type stars covered in our survey. Hence, also for this distinction, it is unclear if it could explain the differences in frequency. Perhaps the most likely explanation is simply that the real frequency is intermediate, in the range of $\sim 2\%$, and that modest statistical fluctuations caused the apparently dissimilar frequencies in the surveys.

We thank the staff at Gemini and ESO for their support during these observations. Our study made use of the CDS and SAO/NASA ADS services. Support for this work was provided by NASA through Hubble Fellowship grant HF-51290.01 awarded by the Space Telescope Science Institute, which is operated by the Association of Universities for Research in Astronomy, Inc., for NASA, under contract NAS 5-26555. Additional support came from grants to RJ from the Natural Sciences and Engineering Research Council of Canada.

REFERENCES

- Ahmic, M., Jayawardhana, R., Brandeker, A., Scholz, A., van Kerkwijk, M.H., Delgado-Donate, E., & Froebrich, D. 2007, *ApJ* 671, 2074
- Allard, F., Hauschildt, P., Alexander, D.R., Tamanai, A., & Schweitzer, A. 2001, *ApJ* 556, 357
- Artigau, E. et al. 2008, *SPIE* 7014, 66
- Baraffe, I., Chabrier, G., Allard, F., & Hauschildt, P. 1998, *A&A* 337, 403
- Baraffe, I., Chabrier, G., Barman, T., Allard, F., & Hauschildt, P. 2003, *A&A* 402, 701
- Babu, G.J. & Feigelson, E.D. 2006, in *Astronomical Society of the Pacific Conference Series*, Vol. 351, *Astronomical Data Analysis Software and Systems XV*, ed. C. Gabriel, C. Arviset, D. Ponz, & S. Enrique, 127
- Bouy, H., Brandner, W., Martin, E., Delfosse, X., Allard, F., & Basri, G. 2003, *AJ* 126, 1526
- Brandeker, A., Jayawardhana, R., Khavari, P., Haisch, K.E., & Mardones, D. 2006, *ApJ* 652, 1572
- Burgasser, A., Reid, I.N., Siegler, N., Close, L., Allen, P., Lowrance, P., & Gizis, J. 2007, in *Protostars and Planets V*, ed. B. Reipurth, D. Jewitt & K. Kiel, 427
- Carson, J. et al. 2013, *ApJ* 763, L32
- Chabrier, G., Baraffe, I., Allard, F., & Hauschildt, P. 2000, *ApJ* 542, 464
- Chen, C.H., Mamajek, E.E., Bitner, M.A., Pecaue, M., Su, K.Y.L., & Weinberger, A.J. 2011, *ApJ*, 738, 122
- Chen, C.H., Pecaue, M., Mamajek, E.E., Su, K.Y.L., & Bitner, M.A. 2012, *ApJ*, 756, 133
- Chini, R., Hoffmeister, V.H., Nasser, A., Stahl, O., & Zinnecker, H. 2012, *MNRAS*, 424, 1925
- Cushing, M.C., Rayner, J.T., Vacca, W.D. 2005, *ApJ*, 623, 1115
- Duchêne, G. & Kraus, A. 2013, *ARA&A* accepted, arXiv:1303.3028
- Eggleton, P.P. & Tokovinin, A.A. 2008, *MNRAS*, 389, 869
- Fischer, D. & Marcy, G. 1992, *ApJ* 396, 178
- Goodwin, S.P. 2013, *MNRAS*, 430, L6
- Ireland, M., Kraus, A., Martinache, F., Law, N., & Hillenbrand, L.A. 2011, *ApJ*, 726, 113
- Janson, M., Bergfors, C., Goto, M., Brandner, W., & Lafrenière, D. 2010, *ApJ*, 710, L35
- Janson, M. et al. 2011, *ApJ*, 728, 85
- Janson, M. et al. 2012, *ApJ*, 754, 44

- Janson, M., Jayawardhana, R., Girard, J., Lafrenière, D., Bonavita, M., Gizis, J., & Brandeker, A. 2012, *ApJ*, 758, L2
- Joergens, V. 2008, *A&A* 492, 545
- Kouwenhoven, M.B.N., Brown, A.G.A., Portegies Zwart, S.F., & Kaper, L. 2007, *A&A* 470, 123
- Lafrenière, D., Jayawardhana, R., & van Kerkwijk, M. 2008, *ApJ*, 689, L153
- Lafrenière, D., Jayawardhana, R., Brandeker, A., Ahmic, M. & van Kerkwijk, M. 2008, *ApJ*, 683, 844
- Lafrenière, D., Jayawardhana, R., & van Kerkwijk, M. 2010, *ApJ*, 719, 497
- Lafrenière, D., Jayawardhana, R., Janson, M., Helling, C., Witte, S. & Hauschildt, P. 2011, *ApJ*, 730, 42
- Lagrange, A.-M., et al. 2009, *A&A*, 493, L21
- Lawrence, A., et al. 2007, *MNRAS*, 379, 1599
- Lenzen, R., et al. 2003, *SPIE*, 4841, 944
- Marois, C., Macintosh, B., Barman, T., Zuckerman, B., Song, I., Patience, J., Lafrenière, D., & Doyon, R. 2008, *Science*, 322, 1348
- McGregor, J. et al. 2002, *SPIE*, 4841, 178
- Öpik, E. 1924, *Publ. Obs. Tartu*, 25, 6
- Pecaut, M.J., Mamajek, E.E., & Bubar, E.J. 2012, *ApJ*, 746, 154
- Perryman, M.A.C. et al. 1997, *A&A* 323, 49
- Quiroga, C., Torres, A.F., & Cidale, L.S. 2010, *A&A* 521, 75
- Raghavan, D. et al. 2010, *ApJS* 190, 1
- Rayner, J.T., Cushing, M.C., & Vacca, W.D. 2009, *ApJS*, 185, 289
- Reggiani, M. & Meyer, M.R. 2013, *A&A* accepted, arXiv:1304.3459
- Rizzuto, A.C., Ireland, M.J., & Robertson, J.G. 2011, *MNRAS*, 416, 3108
- Rousset, G., et al. 2003, *SPIE*, 4839, 140
- Siess, L., Dufour, E., & Forestini, M. 2000, *A&A*, 358, 593
- Shatsky, N. & Tokovinin, A. 2002, *A&A*, 382, 92
- Slesnick, C.L., Hillenbrand, L.A., Carpenter, J.M. 2004, *ApJ*, 610, 1045
- Skrutskie, M.F. et al. 2006, *AJ* 131, 1163
- Song, I., Zuckerman, B., & Bessell, M.S. 2012, *AJ*, 144, 8
- Thalmann, C., et al. 2013, *ApJ*, 763, L29
- Vigan, A. et al. 2012, *A&A*, 544, 9
- de Zeeuw, P.T., Hoogerwerf, R., de Bruijne, J.H.J., Brown, A.G.A., & Blaauw, A. 1999, *AJ*, 117, 354

This 2-column preprint was prepared with the AAS L^AT_EX macros v5.2.

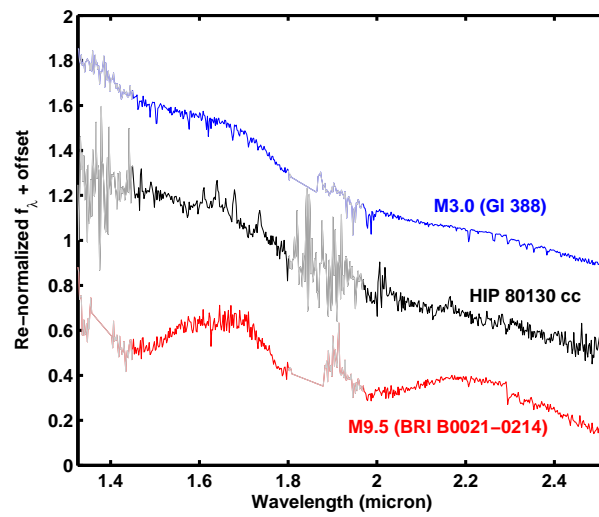


Fig. 5.— Spectrum of the candidate companion to HIP 80130, along with spectral standard stars of spectral types M3V and M9.5V (Cushing et al. 2005; Rayner et al. 2009). The candidate spectrum fits best to an early M-type spectrum such as M3V, and is quite distinct from colder atmospheres such as M9.5V, even though the latter would be much more consistent with its K -band brightness.

Table 1:: Target list.

Target	RA (hh mm ss)	Dec (dd mm ss)	SpT ^a	Dist ^b (pc)	\bar{K} (mag)	Assoc.	Age (Myr)	Stat ^c	Mult ^d
HIP 50083	10 13 30.642	-66 22 22.12	A4	93	4.64	LCC	10	N	N
HIP 50847	10 22 58.126	-66 54 05.31	B8	132	5.31	LCC	10	N	Y
HIP 51991	10 37 20.537	-69 21 45.28	A1	177	8.01	LCC	10	Y	N
HIP 55334	11 19 52.765	-70 37 06.54	F2	86	7.08	LCC	10	Y	N
HIP 56543	11 35 38.011	-50 43 24.50	A5	137	7.77	LCC	10	Y	N
HIP 57238	11 44 09.799	-53 44 54.42	A1	173	8.33	LCC	10	Y	Y
HIP 57595	11 48 27.008	-54 09 18.52	F5	171	8.22	LCC	10	Y	Y
HIP 57710	11 50 07.189	-49 32 35.55	A3	119	7.75	LCC	10	Y	Y
HIP 57950	11 53 07.998	-56 43 38.14	F2	105	7.28	LCC	10	Y	N
HIP 58075	11 54 35.595	-54 43 57.28	F2	159	7.93	LCC	10	Y	N
HIP 58146	11 55 28.844	-62 11 47.19	F2	117	6.83	LCC	10	Y	N
HIP 58167	11 55 43.547	-54 10 50.62	F3	91	7.28	LCC	10	Y	N
HIP 58220	11 56 26.556	-58 49 16.87	F3	105	7.39	LCC	10	Y	Y
HIP 58528	12 00 09.407	-57 07 02.18	F5	90	7.42	LCC	10	Y	Y
HIP 58680	12 02 03.374	-51 49 15.71	A4	190	8.41	LCC	10	Y	N
HIP 58899	12 04 44.470	-52 21 15.69	F3	114	7.35	LCC	10	Y	Y
HIP 58996	12 05 47.483	-51 00 12.14	G2	102	7.31	LCC	10	Y	N
HIP 59084	12 07 00.669	-59 41 40.80	F0	136	7.71	LCC	10	Y	N
HIP 59481	12 11 58.825	-50 46 12.48	F3	117	7.51	LCC	10	Y	N
HIP 59505	12 12 12.012	-54 13 49.49	A9	109	7.70	LCC	10	Y	N
HIP 59693	12 14 28.644	-47 36 46.16	F6	119	8.30	LCC	10	Y	Y
HIP 59716	12 14 50.713	-55 47 23.59	F5	101	7.28	LCC	10	Y	N
HIP 59724	12 14 56.366	-47 56 54.59	A6	110	7.42	LCC	10	Y	N
HIP 59960	12 17 53.190	-55 58 31.97	F5	92	6.68	LCC	10	Y	N
HIP 60245	12 21 11.720	-48 03 19.24	F2	124	8.00	LCC	10	Y	N
HIP 60348	12 22 24.847	-51 01 34.31	F5	78	7.67	LCC	10	Y	N
HIP 60459	12 23 42.195	-63 52 12.16	A3	98	7.02	LCC	10	Y	N
HIP 60513	12 24 18.290	-58 58 35.30	F3	126	7.46	LCC	10	Y	N
HIP 60567	12 24 54.914	-52 00 15.76	F6	158	8.39	LCC	10	Y	N
HIP 60885	12 28 40.057	-55 27 19.38	G1	142	7.29	LCC	10	Y	Y
HIP 61049	12 30 46.269	-58 11 16.88	F7	100	7.07	LCC	10	Y	N
HIP 61087	12 31 12.647	-61 54 31.55	F6	92	6.74	LCC	10	Y	N
HIP 61684	12 38 42.793	-68 45 49.08	A9	106	7.20	LCC	10	Y	N
HIP 62032	12 42 54.874	-50 49 00.07	F0	169	7.90	LCC	10	Y	Y
HIP 62134	12 44 01.928	-53 30 20.53	F2	126	7.71	LCC	10	Y	N
HIP 62171	12 44 26.593	-54 20 48.03	F3	114	7.75	LCC	10	Y	N
HIP 62427	12 47 38.703	-58 24 56.74	F8	128	8.12	LCC	10	Y	N
HIP 62657	12 50 19.719	-49 51 48.86	F5	106	7.72	LCC	10	Y	N
HIP 62677	12 50 35.830	-68 05 28.85	F1	183	8.11	LCC	10	Y	N
HIP 63041	12 55 03.916	-63 38 26.79	F0	96	7.14	LCC	10	Y	N
HIP 63272	12 57 57.773	-52 36 54.65	F3	111	7.46	LCC	10	Y	Y
HIP 63435	12 59 56.410	-50 54 35.05	F5	158	7.99	LCC	10	Y	N
HIP 63439	12 59 59.876	-50 23 22.42	F4	135	8.04	LCC	10	Y	N
HIP 63527	13 01 04.365	-53 08 08.48	F1	133	6.86	LCC	10	Y	N
HIP 63836	13 04 59.449	-47 23 48.54	F7	106	7.87	LCC	10	Y	N
HIP 63886	13 05 32.611	-58 32 07.87	F2	102	7.22	LCC	10	Y	N

Table 1:: continued.

Target	RA (hh mm ss)	Dec (dd mm ss)	SpT ^a	Dist ^b (pc)	<i>K</i> (mag)	Assoc.	Age (Myr)	Stat ^c	Mult ^d
HIP 63962	13 06 27.408	-56 52 44.87	G0	211	7.80	LCC	10	Y	N
HIP 64044	13 07 33.502	-52 54 19.85	F5	106	7.51	LCC	10	Y	N
HIP 64184	13 09 16.200	-60 18 30.10	F3	83	7.16	LCC	10	Y	N
HIP 64322	13 10 59.015	-62 05 15.77	F1	106	7.19	LCC	10	N	Y
HIP 64877	13 17 55.420	-61 00 38.84	F5	114	7.41	LCC	10	Y	N
HIP 64995	13 19 19.522	-59 28 20.24	F2	111	7.34	LCC	10	Y	N
HIP 65136	13 20 51.617	-48 43 19.68	F0	162	8.33	LCC	10	Y	N
HIP 65423	13 24 35.130	-55 57 24.24	G3	97	8.08	LCC	10	Y	Y
HIP 65517	13 25 47.838	-48 14 57.74	G2	104	8.08	LCC	10	Y	Y
HIP 65617	13 27 12.195	-59 38 14.23	F8	164	8.36	LCC	10	Y	N
HIP 65875	13 30 08.977	-58 29 04.34	F6	97	6.90	LCC	10	Y	N
HIP 66001	13 31 53.609	-51 13 33.06	G8	167	7.83	LCC	10	Y	N
HIP 67230	13 46 35.397	-62 04 09.64	F5	135	6.89	LCC	10	Y	N
HIP 67428	13 49 09.222	-54 13 42.30	F5	117	7.63	LCC	10	Y	Y
HIP 67497	13 49 54.502	-50 14 23.83	F0	106	7.52	UCL	10	Y	N
HIP 67970	13 55 09.996	-50 44 42.94	F3	111	7.68	UCL	10	Y	N
HIP 68722	14 04 04.926	-37 17 00.78	A7	149	7.72	UCL	10	Y	N
HIP 69291	14 10 59.612	-36 16 01.68	F2	140	7.67	UCL	10	Y	Y
HIP 69302	14 11 04.886	-49 16 23.40	A8	148	7.71	UCL	10	N	N
HIP 69327	14 11 19.987	-54 37 56.06	F0	135	7.71	UCL	10	N	N
HIP 69605	14 14 45.490	-38 22 52.37	A9	200	7.94	UCL	10	Y	N
HIP 69720	14 16 16.986	-53 49 02.15	F0	140	7.86	UCL	10	Y	N
HIP 70149	14 21 11.537	-41 42 24.96	A9	115	8.11	UCL	10	Y	N
HIP 70558	14 25 58.517	-44 49 23.22	F2	122	8.13	UCL	10	Y	N
HIP 71453	14 36 44.131	-40 12 41.61	B8	129	6.02	UCL	10	Y	N
HIP 71498	14 37 19.427	-54 53 50.19	A2	155	8.22	UCL	10	Y	N
HIP 71708	14 40 05.026	-40 54 02.30	A5	129	7.79	UCL	10	Y	Y
HIP 71767	14 40 45.933	-42 47 06.32	F3	193	7.77	UCL	10	Y	Y
HIP 72099	14 44 56.874	-34 22 53.76	F6	157	8.40	UCL	10	Y	Y
HIP 72584	14 50 30.562	-35 05 36.30	A2	173	7.60	UCL	10	Y	N
HIP 72630	14 51 00.664	-36 23 06.50	A9	165	8.45	UCL	10	Y	N
HIP 73147	14 56 55.776	-42 27 40.38	A1	217	7.94	UCL	10	Y	N
HIP 73777	15 04 48.919	-39 49 23.59	F8	94	8.16	UCL	10	Y	N
HIP 73913	15 06 17.952	-35 24 22.27	A9	141	7.83	UCL	10	Y	N
HIP 73990	15 07 14.943	-29 30 16.07	A9	97	7.32	UCL	10	Y	N
HIP 74104	15 08 42.506	-44 29 04.49	A2	168	7.67	UCL	10	Y	Y
HIP 74499	15 13 27.961	-33 08 50.23	F4	114	7.65	UCL	10	Y	N
HIP 74865	15 17 56.113	-30 28 41.49	F3	124	7.81	UCL	10	Y	N
HIP 74959	15 19 05.423	-36 21 44.08	F5	151	8.15	UCL	10	Y	N
HIP 75480	15 25 09.398	-26 34 31.05	F0	136	7.38	UCL	10	Y	N
HIP 75491	15 25 16.053	-38 09 28.64	F3	173	7.43	UCL	10	Y	N
HIP 75683	15 27 42.320	-36 14 13.12	F4	141	8.37	UCL	10	Y	N
HIP 75824	15 29 23.098	-40 09 49.96	F3	152	7.77	UCL	10	Y	N
HIP 75891	15 30 04.278	-41 07 10.16	F2	155	7.57	UCL	10	Y	Y
HIP 75933	15 30 34.047	-38 29 46.32	F3	194	7.72	UCL	10	Y	N
HIP 76084	15 32 20.139	-31 08 33.75	F2	146	7.51	UCL	10	Y	N

Table 1:: continued.

Target	RA (hh mm ss)	Dec (dd mm ss)	SpT ^a	Dist ^b (pc)	<i>K</i> (mag)	Assoc.	Age (Myr)	Stat ^c	Mult ^d
HIP 76501	15 37 27.916	-32 29 06.10	F2	154	7.52	UCL	10	Y	N
HIP 76875	15 41 53.217	-34 53 19.91	F2	97	7.41	UCL	10	Y	N
HIP 77038	15 43 47.639	-35 28 29.88	F3	128	7.92	UCL	10	Y	Y
HIP 77388	15 47 51.175	-38 15 36.09	A6	136	7.40	UCL	10	Y	Y
HIP 77432	15 48 24.788	-42 37 04.97	F5	99	7.87	UCL	10	Y	N
HIP 77502	15 49 31.985	-31 15 39.69	F3	200	7.87	UCL	10	Y	N
HIP 77520	15 49 39.636	-38 46 39.15	F3	131	8.00	UCL	10	Y	Y
HIP 77545	15 49 59.797	-25 09 03.39	A2	111	7.90	US	5	Y	N
HIP 77713	15 51 59.758	-34 49 41.44	F5	136	8.11	UCL	10	Y	N
HIP 77813	15 53 20.898	-19 23 53.58	F8	90	7.30	US	5	Y	N
HIP 77815	15 53 21.926	-21 58 16.54	A5	143	7.22	US	5	Y	Y
HIP 78043	15 56 05.616	-36 53 34.53	F3	172	7.94	UCL	10	Y	N
HIP 78150	15 57 28.548	-50 16 10.66	A7	146	7.21	UCL	10	Y	Y
HIP 78233	15 58 29.305	-21 24 03.97	F2	258	7.69	US	5	Y	N
HIP 78324	15 59 30.880	-40 51 54.57	B9	167	7.49	UCL	10	Y	N
HIP 78384	16 00 07.322	-38 23 48.04	B2	151	4.09	UCL	10	N	N
HIP 78555	16 02 18.532	-35 16 11.74	F0	101	7.73	UCL	10	Y	N
HIP 78641	16 03 13.550	-35 17 14.90	A5	132	7.62	UCL	10	Y	N
HIP 78963	16 07 12.673	-27 05 58.02	A9	169	7.31	US	5	Y	N
HIP 78977	16 07 17.788	-22 03 36.49	F7	114	7.05	US	5	Y	N
HIP 79054	16 08 10.509	-23 51 02.44	F0	126	7.83	US	5	Y	Y
HIP 79083	16 08 35.144	-20 45 29.64	F4	159	6.68	US	5	Y	N
HIP 79097	16 08 43.660	-25 22 36.74	F3	171	7.25	US	5	Y	Y
HIP 79258	16 10 35.957	-32 45 42.78	F3	144	8.21	US	5	Y	N
HIP 79288	16 10 55.110	-25 31 21.41	F0	116	7.88	US	5	Y	N
HIP 79369	16 11 55.519	-21 06 17.99	F0	122	7.56	US	5	Y	N
HIP 79392	16 12 09.894	-23 55 17.54	A2	194	7.54	US	5	Y	Y
HIP 79516	16 13 34.331	-45 49 03.59	F5	127	7.79	UCL	10	Y	N
HIP 79606	16 14 40.161	-20 14 03.00	F6	179	7.07	US	5	Y	N
HIP 79673	16 15 37.144	-41 38 58.56	F2	146	7.84	UCL	10	Y	N
HIP 79710	16 16 03.841	-49 04 29.38	F0	103	7.61	UCL	10	Y	N
HIP 79733	16 16 21.918	-28 09 50.48	A0	249	7.93	US	5	Y	N
HIP 79742	16 16 28.381	-38 44 12.32	F5	141	8.07	UCL	10	Y	N
HIP 79910	16 18 39.147	-21 35 34.18	F3	138	7.54	US	5	Y	N
HIP 79977	16 19 29.237	-21 24 13.25	F2	132	7.80	US	5	Y	N
HIP 80088	16 20 50.226	-22 35 38.73	A9	164	7.79	US	5	Y	N
HIP 80130	16 21 21.148	-22 06 32.26	A9	136	7.37	US	5	N	U
HIP 80208	16 22 27.994	-49 34 20.51	B6	171	5.40	UCL	10	N	N
HIP 80586	16 27 12.528	-27 11 21.96	F5	128	7.19	US	5	Y	N
HIP 81392	16 37 21.670	-30 06 52.19	G2	197	7.78	US	5	Y	N
HIP 81455	16 38 10.816	-29 40 40.20	F5	115	8.04	US	5	Y	N
HIP 81851	16 43 05.389	-26 27 30.80	F2	126	7.51	US	5	Y	N
HIP 82218	16 47 47.338	-19 52 31.98	F2	127	7.80	US	5	Y	N
HIP 82534	16 52 13.311	-26 55 10.86	F0	150	7.37	US	5	Y	N
HIP 82569	16 52 41.719	-38 45 37.30	F3	152	7.56	UCL	10	Y	N
HIP 83159	16 59 42.481	-37 26 16.88	F5	148	7.92	UCL	10	Y	N

Table 1:: continued.

Target	RA (hh mm ss)	Dec (dd mm ss)	SpT ^a	Dist ^b (pc)	<i>K</i> (mag)	Assoc.	Age (Myr)	Stat ^c	Mult ^d
^a Spectral type from SIMBAD, complemented with values from Chen et al. (2012). ^b Distance uncertainty for individual stars is typically $\sim 20\%$ ^c Flag for whether the target is included in the statistical study, (Y)es or (N)o. ^d Flag for whether the target is observed to be multiple by NICI, (Y)es, (N)o, or (U)nclear.									

Table 2:: Candidate astrometry

Target	CC	ΔK^a (mag)	Epoch 1 (MJD)	Sep ^a ($''$)	PA ^a (deg)	Epoch 2 (MJD)	Sep ^a ($''$)	PA ^a (deg)	FAP (%)
HIP 55334	1	9.5	55641.0	3.346	42.2	56053.0	3.347	43.0	9.8
HIP 56543	1	9.0	55641.0	2.736	239.1	55987.2	2.722	238.9	5.4
HIP 56543	2	9.4	55641.0	2.684	242.1	55987.2	2.668	241.8	7.0
HIP 57595	1	7.9	55663.0	3.345	84.5	55987.2	3.373	84.5	7.0
HIP 57595	2	8.1	55663.0	4.966	314.7	55987.2	4.979	315.0	17.0
HIP 58220	1	3.6	55641.2	0.761	315.9	55987.5	0.751	316.3	0.02
HIP 58220	2	10.1	55641.2	2.752	16.7	55987.5	2.748	17.4	33.1
HIP 58220	3	11.8	55641.2	2.887	164.1	55987.5	2.911	163.1	80.8
HIP 58220	4	11.4	55641.2	4.805	197.6	55987.5	4.802	197.0	96.5
HIP 58680	1	8.3	55641.2	4.433	149.8	56020.3	4.456	149.7	13.6
HIP 59481	1	8.0	55641.2	2.213	174.1	55990.2	2.226	173.3	1.1
HIP 59716	1	11.0	55641.2	2.409	160.3	55990.2	2.428	159.5	23.4
HIP 60245	1	11.1	55641.2	2.027	193.6	56020.2	2.023	192.6	16.2
HIP 60348	1	10.5	55641.2	3.809	172.9	56015.2	3.819	172.4	25.5
HIP 60459	1	9.0	55650.0	1.606	75.6	55990.2	1.616	75.3	13.6
HIP 60459	2	9.6	55650.0	2.273	225.3	55990.2	2.250	225.6	38.2
HIP 60459	3	8.5	55650.0	4.547	13.4	55990.2	4.563	13.5	54.2
HIP 60513	1	9.1	55663.0	1.927	284.6	55990.2	1.911	285.6	9.1
HIP 61087	1	6.8	55663.0	1.284	149.4	55990.2	1.249	148.1	1.1
HIP 61087	2	8.5	55663.0	2.383	101.7	55990.2	2.387	100.6	13.1
HIP 61087	3	7.5	55663.0	4.269	107.5	55990.2	4.273	107.0	18.5
HIP 61087	4	9.3	55663.0	2.724	83.3	55990.2	2.744	82.6	29.2
HIP 61087	5	9.8	55663.0	4.890	83.2	55990.2	4.902	82.8	80.9
HIP 62171	1	9.8	55663.0	2.968	289.7	56015.2	2.969	290.3	14.9
HIP 62677	1	7.2	55663.0	1.628	147.9	56020.2	1.645	147.3	2.1
HIP 62677	2	5.8	55663.0	3.317	154.4	56020.2	3.333	154.5	3.1
HIP 62677	3	7.3	55663.0	3.470	220.9	56020.2	3.452	220.6	10.0
HIP 63041	1	9.4	55685.0	1.859	211.4	56020.2	1.844	211.4	32.7
HIP 63041	2	8.5	55685.0	2.468	192.4	56020.2	2.458	192.1	28.9
HIP 63041	3	9.0	55685.0	4.130	136.6	56020.2	4.144	136.4	75.9
HIP 63041	4	7.8	55685.0	2.830	48.3	56020.2	2.843	49.5	22.7
HIP 63836	1	7.2	55695.2	4.964	36.4	55987.2	4.995	36.5	3.5
HIP 63886	1	6.2	55695.2	4.966	29.2	56053.0	5.007	29.4	5.5
HIP 63886	2	9.3	55695.2	4.842	325.0	56053.0	4.853	325.1	43.4
HIP 64184	1	8.6	55725.0	1.480	155.7	55987.2	1.472	155.5	5.0
HIP 64184	2	9.6	55725.0	2.050	345.8	55987.2	2.075	347.1	18.9
HIP 64877	1	9.8	55654.2	2.802	288.6	55987.2	2.768	288.9	57.7
HIP 64995	1	6.8	55654.2	3.264	63.9	55987.2	3.280	63.7	6.0
HIP 65423	1	4.4	55654.2	1.832	247.3	55987.2	1.832	247.6	0.2
HIP 65517	1	4.5	55725.0	0.352	321.9	55987.2	0.354	322.5	0.004
HIP 65617	1	8.3	56024.0	1.237	319.9	56336.5	1.235	320.5	6.9
HIP 65617	2	9.3	56024.0	1.545	53.7	56336.5	1.570	53.7	21.5
HIP 65617	3	8.4	56024.0	1.139	134.0	56336.5	1.147	133.8	6.4
HIP 67230	1	9.7	56024.0	2.866	158.6	56336.5	2.880	158.1	59.6
HIP 67230	2	9.5	56024.0	2.964	126.0	56336.5	2.989	125.7	56.1
HIP 69605	1	10.0	56022.0	2.043	105.1	56339.5	2.065	104.9	4.0

Table 2:: continued.

Target	CC	ΔK^a (mag)	Epoch 1 (MJD)	Sep ^a ($''$)	PA ^a (deg)	Epoch 2 (MJD)	Sep ^a ($''$)	PA ^a (deg)	FAP ^b (%)
HIP 69720	1	10.9	56024.2	4.214	345.9	56336.5	4.230	346.2	75.1
HIP 69720	2	11.9	56024.2	4.690	308.2	56336.5	4.683	308.6	97.5
HIP 70149	1	9.8	56022.0	2.136	185.4	56339.5	2.110	184.9	5.2
HIP 71498	1	8.8	56024.2	3.875	129.3	56339.5	3.870	128.9	41.0
HIP 71498	2	10.5	56024.2	4.438	294.6	56339.5	4.433	294.8	91.6
HIP 72099	1	4.2	55723.2	0.664	33.8	55987.2	0.671	34.4	0.007
HIP 72584	1	10.3	55723.2	2.612	61.7	56020.2	2.635	61.7	5.7
HIP 72630	1	4.3	55677.2	4.350	176.3	55987.2	4.404	176.2	0.3
HIP 72630	2	9.7	55677.2	4.626	184.8	55987.2	4.662	184.5	30.1
HIP 73147	1	7.5	55677.2	4.143	254.2	55987.2	4.098	254.5	4.8
HIP 73147	2	10.2	55677.2	4.200	306.0	55987.2	4.194	306.5	34.2
HIP 73777	1	8.6	55677.2	3.267	24.3	55987.2	3.312	24.3	5.8
HIP 73913	1	10.1	55677.2	3.645	108.5	56013.2	3.672	108.3	17.8
HIP 74959	1	10.3	55715.2	3.095	43.7	56020.2	3.127	43.3	18.7
HIP 74959	2	10.1	55715.2	3.370	229.2	56020.2	3.338	229.7	18.9
HIP 75683	1	9.2	55715.2	2.209	69.8	56005.2	2.211	69.3	5.8
HIP 75683	2	8.9	55715.2	4.232	261.8	56005.2	4.226	262.2	15.9
HIP 75824	1	7.5	55723.2	3.016	36.5	56015.2	3.022	36.9	2.5
HIP 75824	2	11.1	55723.2	4.333	63.4	56015.2	4.338	63.7	56.3
HIP 75891	1	2.5	55723.2	0.438	314.0	55990.2	0.450	312.7	0.001
HIP 75933	2	10.5	55723.2	3.178	2.6	56012.2	3.195	3.5	18.5
HIP 75933	3	12.0	55723.2	4.406	88.5	56012.2	4.433	88.9	69.8
HIP 76501	1	11.1	55723.2	3.229	131.8	56005.2	3.229	132.1	16.8
HIP 76501	2	11.3	55723.2	4.587	279.6	56005.2	4.582	280.2	34.8
HIP 77038	1	3.6	56024.2	1.443	232.3	56335.2	1.437	232.5	0.02
HIP 77038	2	4.5	56024.2	1.429	243.2	56335.2	1.408	243.8	0.05
HIP 77432	1	8.3	55712.2	3.454	159.0	56005.2	3.427	159.1	11.0
HIP 77432	2	8.6	55712.2	1.764	265.8	56005.2	1.777	266.7	3.7
HIP 77432	3	9.5	55712.2	4.264	69.7	56005.2	4.259	69.5	35.7
HIP 77502	1	9.0	56024.2	1.213	59.9	56338.5	1.224	59.6	0.8
HIP 77520	1	1.9	55712.2	2.222	196.7	56053.0	2.225	196.7	0.03
HIP 77520	2	9.7	55712.2	3.535	174.9	56053.0	3.537	174.4	21.4
HIP 77713	1	9.4	55712.2	2.949	62.0	56005.2	2.972	61.8	10.2
HIP 78324	1	10.1	55712.2	3.492	110.9	56005.2	3.492	111.1	29.7
HIP 78555	1	7.6	55712.2	1.954	71.6	56005.2	1.965	70.8	1.2
HIP 78555	2	7.7	55712.2	4.399	185.1	56005.2	4.371	185.1	6.2
HIP 78555	3	10.3	55712.2	3.740	281.9	56005.2	3.751	282.6	29.3
HIP 78555	4	10.4	55712.2	4.368	54.4	56005.2	4.375	54.1	40.0
HIP 78555	5	10.5	55712.2	4.025	106.5	56005.2	4.023	106.1	37.4
HIP 78963	1	9.7	55712.2	4.583	61.3	56005.2	4.573	61.4	13.5
HIP 78977	1	8.7	55712.2	3.739	30.3	56006.2	3.744	30.1	2.5
HIP 79258	1	9.5	55712.2	4.247	98.3	56005.2	4.250	98.2	30.6
HIP 79369	1	10.1	55696.2	2.685	196.2	56005.5	2.655	195.6	5.8
HIP 79516	1	8.6	55696.2	4.585	181.9	56005.2	4.560	181.7	51.5
HIP 79516	2	9.0	55696.2	4.227	337.2	56005.2	4.247	337.7	56.3
HIP 79516	3	8.1	55696.2	4.692	342.5	56005.2	4.719	342.9	40.7

Table 2:: continued.

Target	CC	ΔK^a (mag)	Epoch 1 (MJD)	Sep ^a ($''$)	PA ^a (deg)	Epoch 2 (MJD)	Sep ^a ($''$)	PA ^a (deg)	FAP ^b (%)
HIP 79673	1	8.1	55696.2	2.692	255.4	56005.5	2.674	255.9	8.5
HIP 79673	2	9.7	55696.2	2.561	132.5	56005.5	2.548	131.9	23.8
HIP 79673	3	10.1	55696.2	2.346	147.6	56005.5	2.335	146.9	26.6
HIP 79673	4	10.4	55696.2	2.696	285.7	56005.5	2.694	286.4	40.1
HIP 79673	5	10.5	55696.2	3.374	103.8	56005.5	3.393	103.4	58.0
HIP 79710	1	9.2	55696.2	2.797	282.0	56020.3	2.797	282.9	67.8
HIP 79710	2	9.7	55696.2	2.877	126.8	56020.3	2.880	126.2	82.9
HIP 79710	3	9.5	55696.4	3.463	128.2	56020.3	3.460	127.7	88.8
HIP 79710	4	8.1	55696.4	4.106	54.2	56020.3	4.130	54.0	64.8
HIP 79710	5	10.3	55696.4	3.720	161.1	56020.3	3.691	160.7	99.1
HIP 79710	6	10.1	55696.4	4.862	73.4	56020.3	4.871	73.3	99.9
HIP 79710	7	10.3	55696.4	4.836	82.7	56020.3	4.841	82.5	100.0
HIP 79710	8	5.3	55696.4	3.898	73.6	56020.3	3.920	73.3	10.3
HIP 79742	1	9.8	55675.5	2.658	293.2	56005.5	2.656	293.7	23.3
HIP 80130	1	7.1 ^c	55675.5	4.121	111.0	56338.5	4.117	111.0	1.0
HIP 81851	1	8.9	55675.5	1.632	268.3	56020.3	1.614	269.2	2.4
HIP 81851	2	10.3	55675.5	2.525	4.6	56020.3	2.553	4.9	15.5
HIP 82534	1	10.4	55641.5	3.238	273.2	55989.5	3.240	273.5	36.1
HIP 82534	2	10.4	55641.5	3.135	51.4	55989.5	3.151	51.2	34.3
HIP 82534	3	9.5	55641.5	4.718	38.8	55989.5	4.726	38.7	37.6
HIP 82569	1	8.0	55695.2	4.991	331.2	56336.5	5.010	331.2	52.8
HIP 82569	2	8.5	55695.2	3.109	334.7	56336.5	3.119	334.8	35.0
HIP 82569	3	9.6	55695.2	2.901	8.0	56336.5	2.908	7.8	58.8
HIP 82569	4	10.2	55695.2	3.397	40.6	56336.5	3.393	40.5	85.7
HIP 82569	5	10.6	55695.2	4.419	75.9	56336.5	4.414	76.0	98.9
HIP 82569	6	9.8	55695.2	2.571	278.5	56336.5	2.572	278.7	55.7
HIP 82569	7	9.5	55695.2	1.594	201.2	56336.5	1.603	201.0	21.9
HIP 83159	1	9.9	55695.2	3.016	87.1	56012.2	3.023	86.9	86.6
HIP 83159	2	9.2	55695.2	2.891	276.6	56012.2	2.892	277.1	65.6
HIP 83159	3	10.3	55695.2	4.541	323.5	56012.2	4.560	323.7	99.8
HIP 83159	4	10.3	55695.2	4.494	277.4	56012.2	4.491	277.7	99.8

^aErrors are 0.2 mag in contrast, 13 mas in separation and 0.4–0.7° in position angle.^bFalse Alarm Probability, see text for details.^cStrongly variable, see individual note.

Table 3: Properties of the discovered systems.

Target	Pair	Sep. (")	PA (deg)	ΔK (mag)	a_{proj} (AU)	m_A (M_{sun})	m_B (M_{sun})	q	FAP
HIP 57238	AB	1.180±0.008	264.6±0.4	3.8±0.2	204	1.47	0.14	0.09	4×10^{-4}
HIP 57595	AB	0.142±0.004	251.3±0.9	1.3±0.2	24	1.49	0.99	0.66	8×10^{-7}
HIP 57710	AB	1.170±0.008	264.9±0.4	3.7±0.2	139	1.42	0.12	0.08	1×10^{-4}
HIP 58220	AB	0.760±0.008	315.9±0.4	3.6±0.2	80	1.44	0.14	0.10	2×10^{-4}
HIP 58528	AB	4.460±0.008	161.3±0.4	2.3±0.2	399	1.33	0.30	0.23	2×10^{-3}
HIP 58899	AB	4.218±0.008	258.0±0.4	2.5±0.2	483	1.49	0.44	0.29	9×10^{-4}
HIP 58899	AC	0.263±0.004	233.6±0.9	3.9±0.2	30	1.49	0.12	0.08	1×10^{-5}
HIP 59693	AB	0.427±0.004	170.6±0.9	1.8±0.2	51	1.21	0.37	0.30	6×10^{-6}
HIP 60885	AB	0.894±0.008	317.3±0.4	3.7±0.2	127	2.47	0.24	0.10	1×10^{-4}
HIP 62032	AB	0.309±0.004	127.5±0.9	2.6±0.2	52	1.82	0.51	0.28	6×10^{-6}
HIP 63272	AB	0.290±0.004	167.9±0.9	2.5±0.2	32	1.45	0.38	0.26	4×10^{-6}
HIP 65423	AB	1.835±0.005	247.4±0.2	4.4±0.1	228	1.10	0.07	0.06	2×10^{-3}
HIP 65517	AB	0.350±0.005	321.7±1.4	4.5±0.1	39	1.20	0.06	0.05	3×10^{-5}
HIP 67428	AB	3.563±0.008	327.0±0.4	3.8±0.2	416	1.44	0.11	0.08	3×10^{-3}
HIP 69291	AB	1.477±0.008	334.0±0.4	3.8±0.2	207	1.52	0.15	0.10	1×10^{-4}
HIP 71708	AB	3.450±0.008	73.0±0.4	2.3±0.2	445	1.45	0.44	0.30	4×10^{-4}
HIP 71767	AB	0.382±0.004	313.4±0.9	2.0±0.2	74	2.71	1.04	0.38	4×10^{-6}
HIP 72099	AB	0.667±0.005	34.4±0.4	4.2±0.1	107	1.40	0.10	0.07	6×10^{-5}
HIP 74104	AB	1.847±0.008	210.7±0.4	2.9±0.2	310	2.45	0.49	0.20	3×10^{-4}
HIP 75891	AB	0.437±0.004	314.3±0.9	2.5±0.2	68	2.36	0.61	0.26	1×10^{-5}
HIP 77038	AB	1.439±0.008	232.4±0.4	3.3±0.2	185	1.42	0.16	0.12	2×10^{-4}
HIP 77038	AC	1.426±0.008	243.2±0.4	4.2±0.2	183	1.42	0.09	0.07	4×10^{-4}
HIP 77388	AB	1.223±0.008	13.5±0.4	3.0±0.2	167	1.84	0.39	0.21	8×10^{-5}
HIP 77520	AB	2.217±0.008	196.7±0.4	1.9±0.2	291	1.41	0.50	0.36	3×10^{-4}
HIP 77815	AB	0.463±0.004	218.4±0.9	2.3±0.2	66	1.75	0.90	0.51	4×10^{-6}
HIP 78150	AB	1.631±0.008	111.0±0.4	2.1±0.2	238	2.65	0.92	0.35	7×10^{-4}
HIP 79054	AB	0.313±0.004	106.4±0.9	2.3±0.2	39	1.31	0.71	0.54	3×10^{-6}
HIP 79097	AB	0.814±0.008	340.0±0.4	3.3±0.2	139	1.99	0.75	0.38	3×10^{-5}
HIP 79392	AB	3.650±0.008	128.8±0.4	4.3±0.2	709	1.98	0.56	0.28	1×10^{-3}